Ras and Its Signals Diffuse through the Cell on Randomly Moving Nanoparticles

Barak Rotblat, Ofer Yizhar, Roni Haklai, Uri Ashery, and Yoel Kloog

Department of Neurobiochemistry, George S. Wise Faculty of Life Sciences, Tel Aviv University, Tel Aviv, Israel

Abstract

Spatiotemporal modulation of Ras signaling from different intracellular compartments requires mechanisms allowing Ras and its signals to navigate across cells. Here, we describe one mechanism by which clusters of palmitoylated H-Ras and N-Ras isoforms but not nonpalmitoylated K-Ras diffuse through the cytoplasm, independently of ATP, on fast, randomly moving, small cytosolic nanoparticles ("rasosomes"). Rasosomes forced to diffuse out of live cells and trapped by Ras antibody beads appear as round structures of 80- to 100-nm diameter. Association of H-Ras with rasosomes requires Ras palmitoylation and the hypervariable sequence (hvr) upstream of the palmitoylated cysteines. H-Ras hvr mutants that fail to interact with rasosomes are biologically inactive. Epidermal growth factor stimulation rapidly increases active H-Ras-GTP and phosphorylated extracellular signal-regulated kinase (ERK) on rasosomes. Similarly, rasosomes carrying H-Ras(G12V) but not H-Ras are loaded with active ERK. Thus, the rasosome represents a hitherto unknown particle that enables Ras signal information to spread rapidly across cells. (Cancer Res 2006; 66(4): 1974-81)

Introduction

Ras proteins contribute to malignant transformation in many types of human tumors (1–3). They participate critically in the control of complex and diverse networks of signaling cascades that regulate cell proliferation, differentiation, survival, and death (1, 4). The molecular mechanisms allowing active Ras to elicit diverse, sometimes contradictory, biological effects are not well understood and knowledge of how the output of Ras signals is coordinated is still limited. Recent studies provided evidence that aside of the time dependence of activation, Ras signal output is determined by microlocalization (5–10) and macrolocalization (11) of various Ras isoforms at the plasma membrane, endosomes, Golgi, and endoplasmic reticulum (11–13). Such spatiotemporal modulation of Ras signaling from different intracellular compartments requires mechanisms allowing Ras and its signals to navigate within the cell. Recent studies have already documented a constitutive flux of palmitoylated Ras isoforms from the plasma membrane to the Golgi, which is independent of classic trafficking pathways but depends on depalmitoylation and repalmitoylation of Ras (14–16). The mechanisms that allow Ras to cross the cell remained unknown. Here, we describe one such mechanism showing that palmitoylated Ras proteins and their signal can diffuse in the cell on randomly moving nanoparticles.

Materials and Methods

Plasmids and transfection procedures. The expression vectors green fluorescent protein (GFP), GFP-K-Ras, GFP-N-Ras, GFP-H-Ras, GFP-H-Ras(G12V), GFP-H-Ras(G12V)Δhvr, GFP-H-Ras(G12V)Δ2ala, GFP-H-Ras(G12V)Δ1ala, and GFP-tH have been previously described (5, 7, 17). mRFP-H-Ras was prepared by cloning monomeric red fluorescent protein (mRFP) fragment into the *Age*I/*Xho*I sites of the GFP-H-Ras vector. GFP-VSVG expression vector was a gift from B. Aroeti (The Hebrew University, Jerusalem), AlexaX-transferrin was a gift from M. Horwitz (Tel Aviv University), and GFP-GPI expression vector was a gift from Y. Henis (Tel Aviv University). COS-7, baby hamster kidney (BHK), and HeLa cells were maintained as described (8). Cells (2.5×10^5) were plated on 25-mm diameter glass coverslips and transfected 24 hours after plating. Transfection was done with JetPEI (Plyplus-Transfection, Illkirch, France) according to the manufacturers' instructions, using 2 μg DNA. All cotransfections were carried out with a total of 2 μg DNA at a ratio of 1:1.

Biochemical and immunologic procedures. For isolation of rasosomes, 8×10^5 COS cells were plated in 10-cm dishes, transfected with 6 μg of the indicated GFP-Ras vector, and used 12 hours later. As controls for transfection, replicate transfectants were subjected to determination of GFP-Ras, extracellular signal-regulated kinase (ERK), and phospho-ERK by Western blotting. The transfectants were washed with PBS and then incubated with 0.1% digitonin in PBS or treated with 500 ng/mL of streptolysin-O for 2 to 10 minutes. The medium (containing rasosomes that had diffused out of the cells) was collected and subjected to centrifugation ($20,000 \times g$, 5 minutes, at 4°C) to remove debris. The resulting supernatant was subjected to high-spin centrifugation ($100,000 \times g$, 30 minutes, 4°C), and the pellet was resuspended in PBS. This rasosome-enriched preparation (REP) was used for characterization of the rasosomes. Protein-A–coated beads (Dynabeads, Dynal Biotech, Oslo, Norway) were incubated with anti-Ras or anti-GFP antibodies (pan-ras, Calbiochem, La Jolla, CA; anti GFP, Santa Cruz Biotechnology, Santa Cruz, CA) or with naive mouse IgG for 1 hour at room temperature and then incubated with REP overnight at 4°C. They were then washed with PBS and subjected to fluorescence imaging and high-resolution scanning electron microscopy (SEM) or immunoprecipitated and analyzed by Western blotting using anti-ERK or anti–phospho-ERK antibodies, as described (5). To examine the effects of epidermal growth factor (EGF) stimulation on Ras-GTP or phospho-ERK in rasosomes, GFP-H-Ras transfectants were first serum starved for 3 hours and then stimulated with 100 nmol/L EGF for 3 minutes. REPs were prepared as described above and used for GST-RBD pull-down assay, as described (5). The EGF-induced increase in phospho-ERK was determined in a similar manner, except that the REPs were subjected to immunoprecipitation followed by Western blotting, as described above. High-resolution SEMs were done using a JSM-6700F microscope.

Live cell imaging. GFP-expressing cells were transferred to an inverted Olympus IX-70 microscope equipped with a total internal reflection fluorescence (TIRF) condenser (TILL Photonics, Planegg, Germany). Excitation light at 473 and 532 nm was provided by two solid-state lasers (Laser Quantum, Stockport, United Kingdom) coupled into a single optical

Note: Supplementary data for this article are available at Cancer Research Online (http://cancerres.aacrjournals.org/).

B. Rotblat and O. Yizhar contributed equally to this work.

Y. Kloog is an incumbent of The Jack H. Skirball Chair in Applied Neurobiology.

Requests for reprints: Yoel Kloog, Department of Neurobiochemistry, The George S. Wise Faculty of Life Sciences, Tel Aviv University, 69978 Tel Aviv, Israel. Phone: 972-3-640-9699; Fax: 972-3-640-7643; E-mail: yoelk@tauex.tau.ac.il.

doi:10.1158/0008-5472.CAN-05-3791

fiber that was connected to the TIRF condenser (TILL Photonics). Except where otherwise indicated, all experiments were done 24 hours after transfection. During the experiments, the cells were constantly perfused with fresh physiologic saline containing 140 mmol/l NaCl, 2 mmol/l $CaCl_2$, 1 mmol/L $MgCl_2$, 10 mmol/L HEPES, and 2 mg/mL glucose. Unless otherwise stated, all experiments were carried out at room temperature. Time-lapse imaging was done with a CoolSNAP HQ camera (Roper Scientific, Tucson, AZ) controlled by MetaMorph software (Universal Imaging, Downingtown, PA). Except where otherwise indicated, images were obtained every 100 milliseconds. Dual-wavelength imaging was done by inserting a beamsplitter module (DualView, Optical Insights, Santa Fe, NM) between the microscope side port and the camera, which was equipped with filter sets for GFP and rhodamine.

Experiments with brefeldin A were done as follows: 2 hours after transfection with GFP-H-Ras, before any fluorescence was observed in the cells, brefeldin A (10 μg/mL) was added to the medium. By 6 hours after transfection, some of the cells had begun to express the fluorescent proteins, and the cells were then imaged. To label endocytosed membrane, cells were incubated overnight with a low concentration (1 μmol/L) or for 20 minutes with a high concentration (10 μmol/L) of SynaptoRed C2M (equivalent to FM5-95, Biotium, Hayward, CA). ATP depletion in GFP-H-Ras and in RFP-NPY transfectants was obtained by the use of a medium containing 50 mmol/L 2-deoxyglucose and 10 mmol/L NaN_3, as previously described (18). To inhibit protein palmitoylation, we incubated the cells with 50 μmol/L 2-bromopalmitate for 2 hours before imaging. Protein synthesis was blocked by incubation of cells with 50 μg/mL cycloheximide for at least 2 hours before imaging. Golgi GFP-H-Ras was identified by colocalization with the Golgi β-coatomer protein (β-COP; ref. 19) marker using anti-β-COP antibodies and Cy3-labeled secondary antibodies. Cytochalasin D (10 μg/mL, 15-minute incubation) and nocodazole (5 μmol/L, 2-hour incubation) were used to disrupt the actin cytoskeleton and microtubules, respectively.

Tracking of single rasosomes in time-lapse recordings. To obtain an estimate of the size of the GFP-H-Ras rasosomes, we compared their intensity profile with that of subresolution (200-nm diameter) fluorescent beads immobilized on a glass coverslip. The mean intensity profiles were obtained by performing line scans through the intensity maxima of individual fluorescent objects and normalizing to the maximum intensity in each object.

To facilitate particle recognition of single rasosomes, image stacks were spatially high-pass filtered to remove spatial frequencies of >1 μm. Single rasosomes observed in the image stacks were tracked using a custom-written program, and the *X,Y* position of each particle was determined for every frame. Tracking of each particle yielded a trajectory, from which the mean square displacement (MSD ref. 20) in the *XY* plane was extracted as follows:

$$MSD(n\delta t) = \frac{1}{N-n}\sum_{j=1}^{N-n}\{[x(j\delta t + n\delta t) - x(j\delta t)]^2 + [y(j\delta t + n\delta t) - y(j\delta t)]^2\}$$

where δt is the time interval between frames, N is the total number of images in the sequence, and n and j are positive integers with $n = 1, 2, \ldots, (N-1)$. The diffusion coefficient (D) for each tracked particle is obtained by $D = S/4$, where S is the slope of a linear least-squares fit to the MSD plot.

Calculation of global mobility in the submembrane region. To estimate the global degree of mobility within cells imaged using TIRF microscopy, image stacks from time-lapse recordings were temporally high-pass filtered. The filtered image, represented by the matrix $B(j\delta t)$, was obtained by the following calculation:

$$B(j\delta t) = Abs\left\{A(j\delta t) - \frac{1}{10}\sum_{i=0}^{9} A[(j+i)\delta t]\right\}$$

where δt is the time interval between frames, j is the frame number (a positive integer with $j = 1, 2, \ldots, N-10$), and $A(j\delta t)$ is a matrix containing the pixel intensities of the original stack at time $j\delta t$. As a result of this procedure, bright pixels exist in the filtered images $B(j\delta t)$, only where objects transiently appeared in the original stack. To obtain a single representation for the mobility observed during the entire duration of imaging, a SD image was constructed in which each pixel represents the SD of pixel intensities at the same coordinates across the entire time series. The mobility factor calculated from each SD image is its "Shannon entropy." The image entropy, a concept derived from information theory, represents the amount of information contained in an image and is expressed in units of bits/pixel (21). The Shannon entropy of the SD image is calculated by:

$$H(z) = -\sum_{j=1}^{J} P(a_j) z \log P(a_j)$$

where J is the total amount of gray levels contained in the image and $P(a_j)$ is the fraction of pixels containing intensity $P(a_j)$ (21). By employing this calculation, we were able to describe the overall degree of mobility within each cell in terms of a single variable, mobility factor. All algorithms were implemented with Matlab 7 (MathWorks, Natick, MA). Statistical comparisons of mobility factors under different conditions were carried out with a two-tailed Mann-Whitney test.

Results and Discussion

Live cell imaging detects mobile GFP-H-Ras nanoparticles. We used TIRF microscopy and fast time-lapse imaging to track the mobility of GFP-tagged Ras isoforms near the plasma membrane of live cells. TIRF microscopy allowing excitation of fluorophores located within ~250 nm from the plasma membrane (evanescence field; ref. 22) showed that in GFP-H-Ras–transfected BHK cells, GFP-H-Ras was not distributed homogeneously on and near the plasma membrane (Fig. 1*A*); rather, it was found in diffraction-limited spots or particles (<200 nm) that appeared in addition to the diffuse staining originating from membrane-bound GFP-H-Ras (Fig. 1*B-C*). This suggested that each such particle contains multiple GFP-H-Ras molecules. Such particles were detectable as early as 6 hours after transfection (when GFP-H-Ras expression levels were low; Fig. 1*E*) and were not detectable in cells transfected with GFP (Fig. 1*A*), clearly indicating that they do not represent clusters of overexpressed Ras or of GFP molecules. Time-lapse imaging showed that most (but not all) of the GFP-H-Ras clusters are highly mobile and move rapidly in and out of the evanescent field (Supplementary Video S1). Similar fluorescent clusters were viewed in the same cells under epifluorescence in the cytoplasm (Fig. 1*A*; Supplementary Video S2) and in the cytoplasm of cells expressing a nondimerizing GFP variant (23), mRFP (Fig. 1*D*). Destabilization of the Golgi by brefeldin A had no effect on their appearance, indicating that the highly mobile GFP-H-Ras clusters (unlike Ras-carrying Golgi derived vesicles; ref. 24) do not depend on Golgi (Fig. 1*E*).

We then did dual wavelength time-lapse imaging in the cytoplasm of cells cotransfected with GFP-H-Ras and neuropeptide Y (NPY) tagged with mRFP (mRFP-NPY). The latter served as a marker of Golgi-derived vesicles (25). The mRFP-NPY–labeled vesicles did not overlap the rapidly moving GFP-H-Ras particles (Fig. 1*E*). Similar results were obtained in GFP-H-Ras transfectants in which endocytosed membranes were labeled with the fluorescent lipid probe SynaptoRed (ref. 26; Fig. 1*E*) or with Lysotracker Red, a marker of acidic vesicles (ref. 27; data not shown). These findings showed that the GFP-H-Ras particles do not represent typical Golgi-derived or plasma membrane–derived vesicles.

GFP-H-Ras nanoparticles diffuse randomly in the cytoplasm and become immobilized at the plasma membrane. Next, we tracked single GFP-H-Ras particles in the TIRF plane (Fig. 2*A*) and

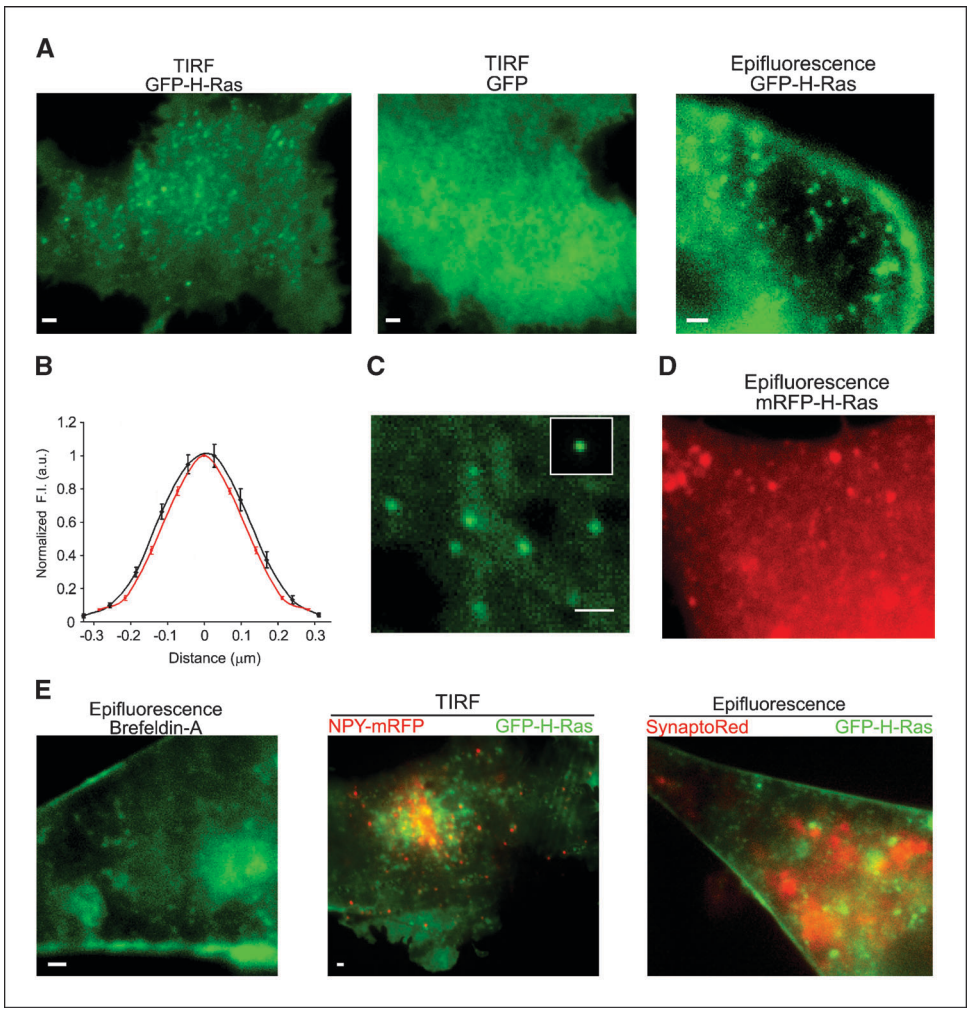

Figure 1. GFP-H-Ras is found on diffraction-limited nanoparticles on the membrane and in the cytoplasm. *A,* live-cell imaging of BHK cells expressing GFP-H-Ras (*left*) or GFP (*middle*) under TIRF, or expressing GFP-H-Ras under epifluorescence in the cytoplasm (*right*). *B, points,* normalized mean fluorescence profile of GFP-H-Ras rasosomes (black, $n = 15$) compared with the mean fluorescence profile of 200-nm fluorescent beads ($n = 5$); *bars,* SE. *X axis,* distance from the location of peak fluorescence intensity. *C,* single GFP-H-Ras particles are visible as fluorescent spots; membrane-bound GFP-H-Ras is seen as diffuse staining. *Inset,* TIRF microscopy image of a 200-nm fluorescent bead immobilized on a glass coverslip. Bar, 1 μm (applies to both images). *D,* live-cell imaging of BHK cells expressing mRFP-H-Ras under epifluorescence in the cytoplasm. *E,* live cell image of a BHK cell transfected with GFP-H-Ras, treated with brefeldin A (*left*), and dual color images of GFP-H-Ras particles tagged with NPY-RFP (*middle*) or stained with SynaptoRed (*right*).

in the cytoplasm and determined their trajectories of lateral motion (Fig. 2*B*). Calculation of the MSD, based on these trajectories, enabled us to characterize the motion of the particles (refs. 28–30; Materials and Methods). The MSD plot of cytoplasmic GFP-H-Ras particles was well fitted by a straight line, indicative of random diffusion (ref. 20, Fig. 2*C*). We also found that cytochalasin D and nocodazole (data not shown), which, respectively, disrupt the actin cytoskeleton and microtubules (both required for directed movement), did not alter the mobility of the GFP-H-Ras particles. Together, these results show that Ras can diffuse through the cytoplasm on randomly moving particles. Importantly, the MSD plot of membrane-proximal particles (in the TIRF plane) exhibited negative curvature (Fig. 2*C*). This indicated that the mobility of the membrane-proximal GFP-H-Ras particles is more restricted than that of the cytoplasmic particles (ref. 20; Fig. 2*C*). This contention was supported by our observation that the mobile particles arriving from the cytoplasm frequently became immobilized at the plasma membrane for extended periods (Fig. 2*D*). Consistently with these observations, the diffusion coefficients (D) of the GFP-H-Ras particles in the TIRF plane ranged from 10^{-5} $\mu m^2/s$ (virtually immobile) to 10^{-2} $\mu m^2/s$ (fast diffusion), whereas the diffusion coefficients of cytoplasmic particles were narrowly distributed between 10^{-2} to 10^{-1} $\mu m^2/s$ (Fig. 2*E*). Importantly, the D value of GFP-H-Ras particles in the TIRF plane (i.e., near and at the plasma membrane) was at least one order of magnitude lower than the D values of membrane-associated single H-Ras molecules, as determined by single-molecule tracking (9, 10) or by fluorescence recovery after photobleaching (5, 6, 8). We hypothesize that the GFP-H-Ras particles at the plane of the membrane might represent part of the immobile fraction documented in these early studies.

To compare the diffusive behavior of GFP-H-Ras particles in COS cells with that of known transport vesicles, we tracked the movement of GFP-VSVG–labeled vesicles traveling from the Golgi to the plasma membrane (31) and of vesicles labeled with Alexa 546–tagged transferrin (endocytosis marker; ref. 32) in COS cells. We found that both Golgi-derived and endocytosed vesicles moved primarily in a directed manner. The D values calculated were, respectively, $2.3 \times 10^{-2} \pm 6.8 \times 10^{-3}$ $\mu m^2/s$ (mean ± SE, $n = 10$) and $4.17 \times 10^{-2} \pm 8.9 \times 10^{-3}$ $\mu m^2/s$ (mean ± SE, $n = 24$) for GFP-VSVG–labeled and transferrin-labeled vesicles. Thus, the mobility of typical transport vesicles is significantly lower than that of the cytoplasmic GFP-H-Ras particles (Fig. 2*E*). These results, along with the observed insensitivity of mobile GFP-H-Ras particles to cytoskeleton-disrupting agents, distinguished the GFP-H-Ras particles from other well-known (28, 29) mobile cytoplasmic objects. Taken together, our experiments suggested that these unique particles represent nanometric objects carrying multiple GFP-H-Ras molecules. We termed these clusters "rasosomes." Rasosomes were detected not only in GFP-H-Ras–transfected BHK

cells (Fig. 1) but also in similarly transfected Rat-1, COS, and HeLa cells (data not shown), indicating that they are not cell type specific.

Rasosomes diffusion is ATP independent. Although single-particle tracking enabled us to determine the uniqueness of the GFP-H-Ras rasosomes and their biophysical properties, it did not allow us to quantify the movement of the entire population of rasosomes appearing transiently in an image sequence above the background fluorescence (indicated by diffuse membrane staining and immobile clusters). Such depiction was needed for quantitative determination of the rasosomes and their relevance to Ras biology. We therefore developed a time-lapse image-processing procedure (see Materials and Methods), which enabled us to calculate the overall mobility of fluorescent objects in image sequences (defined as the "mobility factor"). We constructed a SD image in which each pixel represents the SD of pixel intensities at the same coordinates across the entire time series (see Materials and Methods). In cells with diffuse fluorescence (e.g., cells expressing GFP), the SD image contained relatively uniform pixel values resulting from small variations in fluorescence (Fig. 3*A, bottom*). However, cells with mobile fluorescent objects (e.g., cells expressing GFP-H-Ras) produced SD images with high pixel values at the location in which the mobile objects appeared (Fig. 3*A, top*). The SD image was then quantified to yield a single variable of the overall fluorescence variability defined as the mobility factor (see Materials and Methods). We first tested the validity of this tool by applying it to image sequences of BHK cells expressing NPY-mRFP (Supplementary Fig. S3c). By depleting the cells of ATP, we halted the motion of fluorescently labeled vesicles in these cells and calculated the changes in mobility factors before and after ATP depletion. The mobility factors of ATP-depleted cells gradually declined with time from 3.5 at 0 time to 2.9 at 20 minutes (Fig. 3*B*), a time point at which directed vesicles movement was completely halted. These findings validated the mobility factor as a quantitative measure of fluorescent object mobility and provided biological significance to the mobility factor values. Next, we compared the mobility factors of image sequences of GFP-expressing cells with those of GFP-H-Ras transfected cells. Mobility factor values in the GFP-H-Ras transfectants were significantly higher than in the GFP transfectants (mean, 3.5 $\pm$ 0.15; n = 11 and mean, 2.8 $\pm$ 0.12; n = 8, respectively; Fig. 3*C* and *D*). Using this tool, we next found that neither ATP depletion (Fig. 3*D*) nor low temperature (16°C; data not shown), both of which block vesicular transport (33), had any effect on the mobility factor of GFP-H-Ras rasosomes. The appearance of these rasosomes was also independent of newly synthesized proteins, as shown by the finding that cycloheximide had no effect on their mobility factor (Fig. 3*D*).

Rasosomes carry constitutively active palmitoylated GFP-Ras proteins. Having observed that GFP-H-Ras rasosomes diffuse rapidly through the cytoplasm, we postulated that they operate as diffusible carriers of active Ras. Consistent with this possibility were the findings that constitutively active GFP-H-Ras(G12V), an active form of H-Ras, is also carried on rasosomes (Fig. 3*C* and *E*). These results suggested that interactions of H-Ras with rasosomes might depend not only on the H-Ras

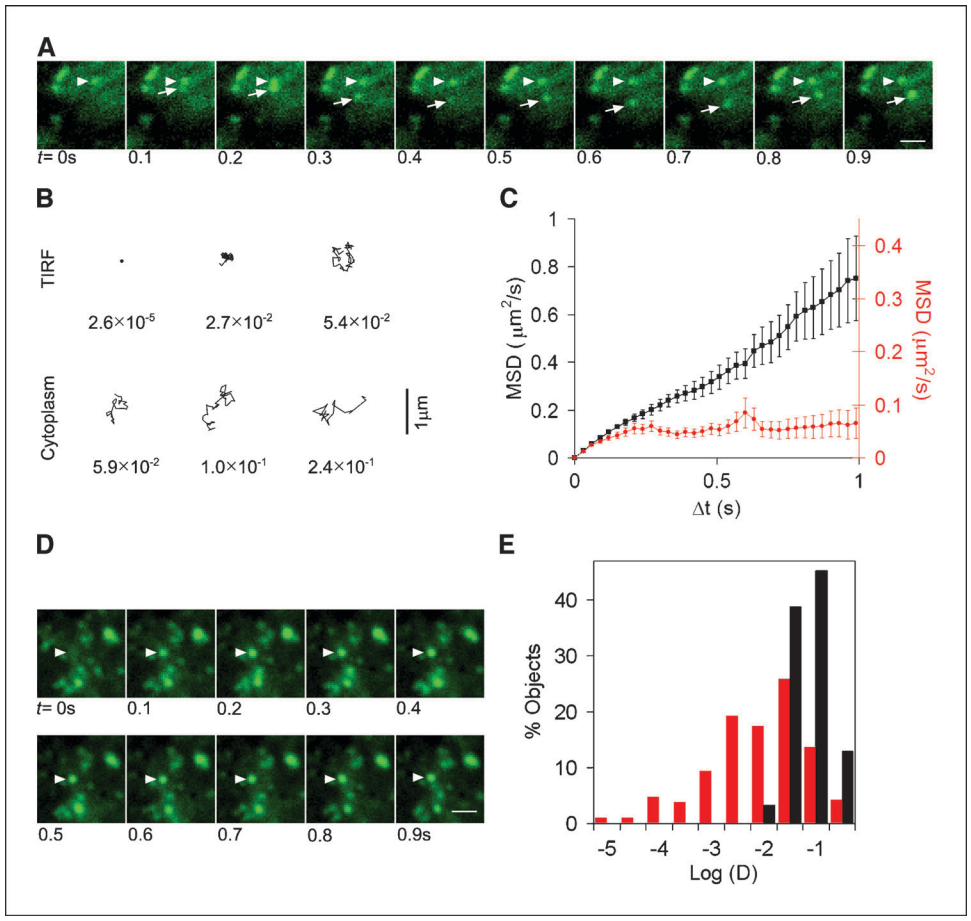

Figure 2. GFP-H-Ras moves in the cytoplasm on freely diffusing nanoparticles. *A,* image sequence of a BHK cell expressing GFP-H-Ras. *Arrows,* single mobile particle; *arrowheads,* single immobile particle. *B,* typical trajectories and diffusion coefficients (*D*) of GFP-H-Ras particles (rasosomes) under TIRF (*top*) and under epifluorescence (*bottom*) illumination. *C, points,* MSD of single GFP-H-Ras particles viewed in the TIRF plane (*red, n* = 246) and in the cytoplasm (*black, n* = 35) of live BHK cells; *bars,* SE. *D,* immobilization of a rasosome (*arrow*) at the cell membrane. Bar, 1 μm. *E,* distribution of diffusion coefficients calculated for cytoplasmic GFP-H-Ras particles (*black columns*) membrane-proximal particles viewed with TIRF (*red columns*).

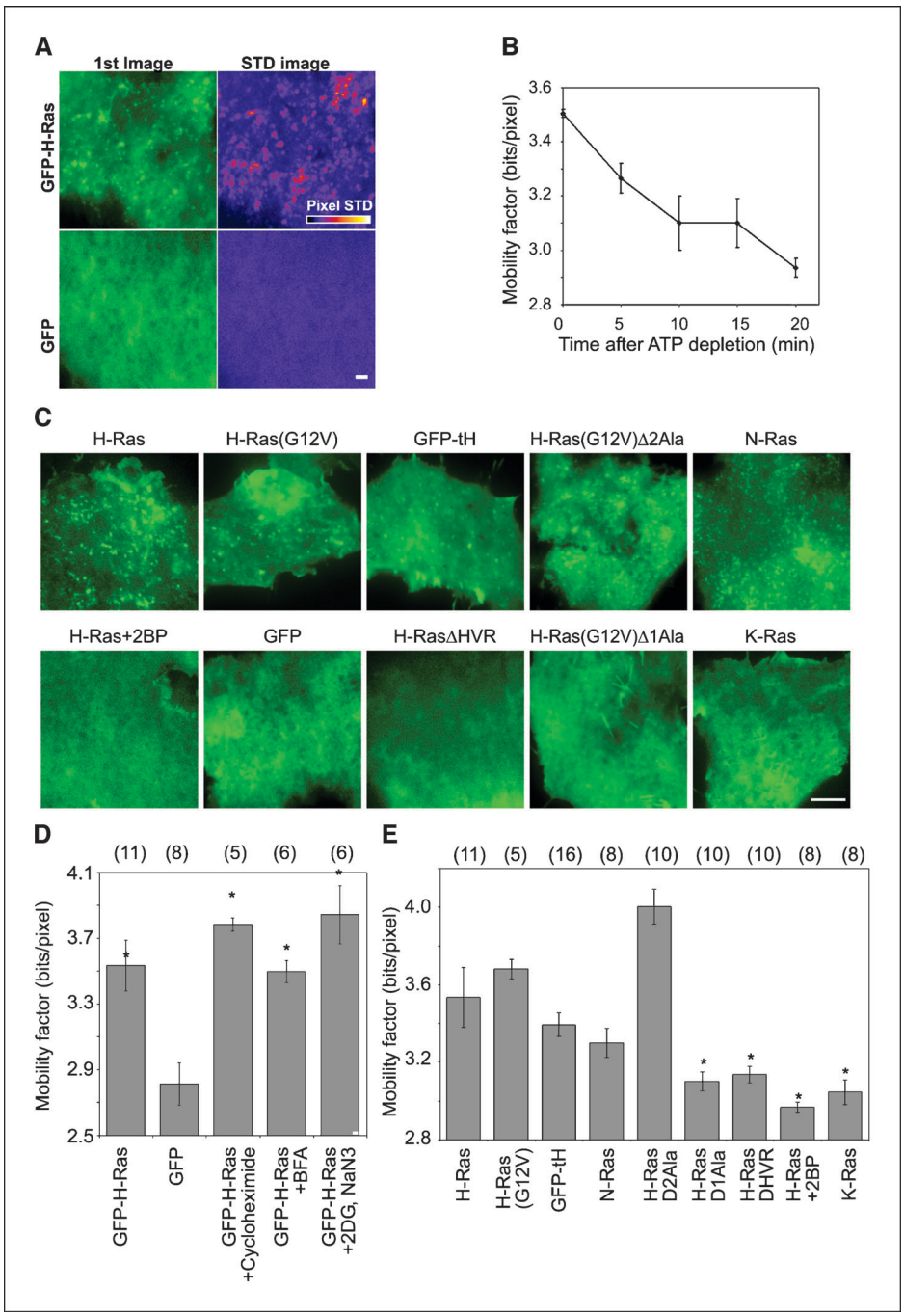

Figure 3. Factors determining rasosome mobility and Ras-rasosome interactions. *A,* the first image of each sequence of live cell TIRF imaging of BHK cells expressing GFP-H-Ras or GFP (*left*). SD image (*STD*) images provide a spatial representation of the movements of fluorescent objects in the entire image sequence. The images are rendered in pseudocolor, where dark blue represents low SD and white represents high SD. *B,* mobility factor as quantitative measure of fluorescent object mobility in live cells. Image sequences of BHK cells expressing NPY-mRFP were collected at before (0 time) and at the indicated times after treatment with 2-deoxyglucose (*2DG*) and NaN_3 (ATP depletion). This resulted in a time-dependent inhibition of NPY-mRFP–labeled vesicle mobility. The image sequences collected at each time point were used to calculate the mobility factors. *C,* first images, as in *A,* of BHK cells expressing the indicated GFP-tagged proteins. Bar, 5 μm. *D,* rasosome mobility is independent of protein synthesis and ATP. *Columns,* mean mobility factors of rasosomes (*n* is denoted in brackets) in BHK cells expressing GFP or GFP-H-Ras and treated as indicated; *bars,* SE. *, $P < 0.005$, compared with GFP (Mann-Whitney test). *E,* biologically inactive H-Ras is excluded from rasosomes. *Columns,* mean mobility factors of rasosomes (*n* is denoted in brackets) in BHK cells expressing the GFP-tagged proteins as indicated; *bars,* SE. *, $P < 0.05$, compared with GFP-H-Ras (Mann-Whitney test).

NH_2-terminal GTPase domain but also on the COOH-terminal hvr linker domain (amino acid residues 167-179) and/or on the downstream lipid anchor that contains two palmitoylated cysteines and a COOH-terminal farnesyl cysteine carboxymethyl ester (34).

To determine whether the hvr domain of H-Ras is required for the latter's interaction with rasosomes, we transfected BHK cells with a GFP-H-Ras(G12V)ΔHVR mutant that lacks the hvr domain but contains the lipid anchor (7). No rasosomes were detectable in GFP-H-Ras(G12V)ΔHVR transfectants (mobility factor = 3.1 ± 0.04, Fig. 3*C* and *E*). This finding indicated that the hvr domain is important for interaction of GFP-H-Ras(G12V) with rasosomes; it also showed that within the context of the GFP-H-Ras(G12V)ΔHVR protein, the lipid anchor by itself might not target Ras to the rasosome. We examined this latter possibility in BHK cells transfected with the GFP-tagged lipid anchor of H-Ras (GFP-tH; ref. 8). These transfectants, however, exhibited ample numbers of GFP-tH rasosomes with high mobility factors (Fig. 3*C* and *E*), indicating that the lipid anchor of H-Ras when separated from the full-length protein provides sufficient force for interactions with rasosomes. Taken together, these results are consistent with the possibility that the NH_2-terminal domain of H-Ras weakens the interactions of GFP-H-Ras(G12V)ΔHVR with the rasosome. It is important to note that GFP-H-Ras(G12V)ΔHVR, which does not interact with rasosomes (Fig. 3*C* and *E*), lacks biological activity, as indicated by its inability to

induce either PC12 cell differentiation (17) or the loss of stress fibers in COS-7 cells (8). This observation strongly suggested that rasosomes are players in the biological activity of H-Ras. To verify this possibility, we used two GFP-H-Ras(G12V) hvr mutants, one of them biologically active [H-Ras(G12V)Δ2Ala] and the other biologically inactive [GFP-H-Ras(G12V)Δ1Ala; refs. 8, 17]. Rasosomes were detectable only in cells expressing the biologically active mutant (Fig. 3*C* and *E*).

Palmitoylation-dependent interaction of GFP-H-Ras with rasosomes. Next, we investigated the significance of palmitoyl moieties in the anchor domain of H-Ras for its interactions with rasosomes. We transfected BHK cells with GFP-H-Ras and then treated the tranfectants with 2-bromopalmitate, an inhibitor of palmitoyl transferase (35). Time-lapse imaging under TIRF illumination showed a strong decrease in the mobility factor of GFP-H-Ras in the 2-bromopalmitate–treated cells; GFP-H-Ras rasosomes were barely detectable in these cells (Fig. 3*C* and *E*). Similar results were obtained in BHK cells transfected with activated GFP-H-Ras(G12V) (data not shown). Thus, Ras association with rasosomes evidently requires palmitoylation. GFP-K-Ras, a nonpalmitoylated Ras isoform (34), was indeed found not to be associated with rasosomes (Fig. 3*C* and *E*). For association of Ras with rasosomes, a single palmitoyl moiety (as in the monopalmitoylated GFP-N-Ras protein; ref. 34) seems to be sufficient (Fig. 3*C* and *E*).

Earlier studies have shown that the palmitoyl residues of Ras proteins are important for trafficking, microlocalization, and signaling of Ras (14–16). These activities were regulated by an acylation/deacylation cycle (14). It is therefore of interest to compare those results with the present findings in connection with rasosomes. First, translocation of H-Ras from plasma membrane to Golgi was found in the earlier study to be blocked by 2-bromopalmitate (14), and in the present study, 2-bromopalmitate inhibited the interaction of GFP-H-Ras with rasosomes (Fig. 3*C* and *E*). Second, tH, H-Ras, and H-Ras(G12V) underwent rapid plasma membrane-to-Golgi translocation (14), and all three are also carried on rasosomes (Fig. 3*C* and *E*). Third, plasma membrane-to-Golgi translocation was not affected by low temperature (16°C), cycloheximide, or inhibitors of endocytosis (14); likewise, none of these treatments affected GFP-H-Ras–rasosome mobility. These common features raise the possibility that rasosomes can participate in the translocation of H-Ras from the plasma membrane to the Golgi (14). Consistent with this possibility are the findings that, unlike vesicles labeled with mRFP-NPY, both rasosome mobility and the rapid translocation of GFP-H-Ras to the Golgi are independent of ATP (Supplementary Fig. S3). In addition, we found that GFP-H-Ras(G12V)Δ2Ala (which is carried on rasosomes) but not GFP-H-Ras(G12V)Δ1Ala (not carried on rasosomes) was enriched in Golgi (Supplementary Fig. S3).

Rasosome isolation and capture on beads coated with Ras antibody. To further study the rasosomes and determine whether they function as platforms for singling, it was necessary to develop ways to isolate them physically and characterize them biochemically. We first used COS cells expressing GFP-H-Ras and treated them with 0.1% digitonin or with streptolysin-O, both of which form small pores in the cell membrane (36). We then used time-lapse imaging under epifluorescence to track GFP-H-Ras particles at 0 time and during digitonization. Digitonin treatment resulted in the rapid appearance (within 2 minutes) of GFP-H-Ras particles in the medium (Fig. 4*A*; see also Supplementary Video S4 online). Similar results were obtained when permeabilization was done with streptolysin-O (data not shown). These findings raised the possibility that the GFP-H-Ras particles observed in the medium represent rasosomes that have diffused out of the cells through the pores formed in the plasma membrane. Several lines of evidence support this possibility. First, GFP-Ras–labeled particles were not detected in the medium of digitonized GFP-H-Ras(G12V)Δ1ala expressing cells (data not shown). GFP-H-Ras(G12V)Δ1ala is stably associated with the plasma membrane (8). This observation indicates that the GFP-H-Ras(G12V) particles observed in the medium of the

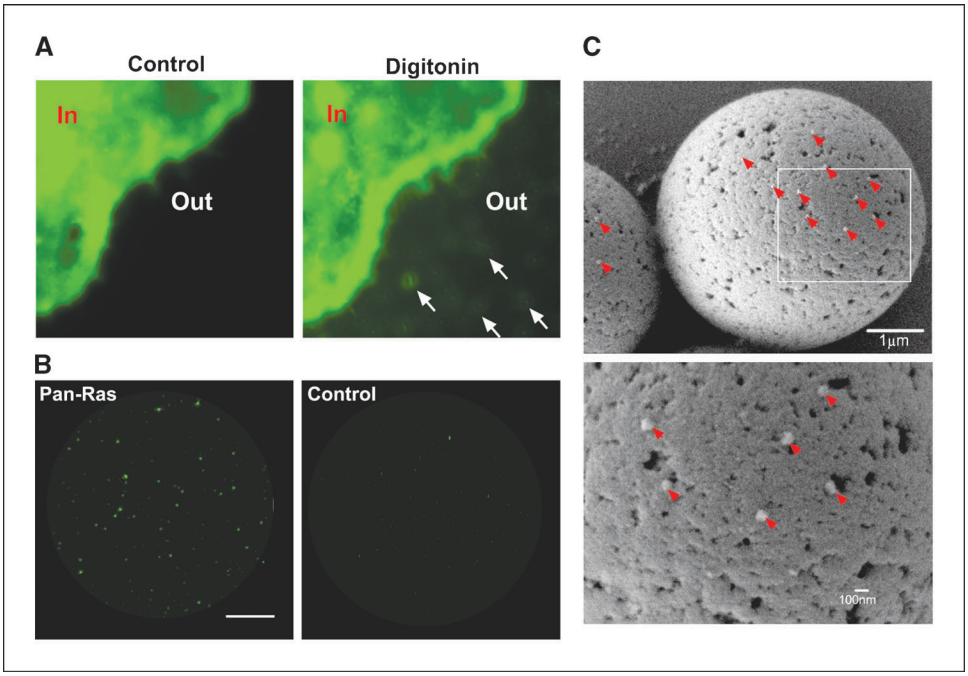

Figure 4. Isolation and ultrastructural characterization of rasosomes. *A,* GFP-H-Ras–transfected COS cells were permeabilized with digitonin and then imaged by epifluorescence. Rasosomes that diffused out of the cells are marked with arrows. *B,* REPs of GFP-H-Ras(G12V) were trapped on anti-Ras antibody beads (*left*) or naive mouse IgG beads (*right*) and then imaged by epifluorescence microscopy. Typical images. Bar, 1 μm. *C,* high-resolution SEM images of anti-ras beads incubated with a REP. Rasosomes on the bead (*arrows*). *Bottom,* region marked with a white rectangle, viewed at higher magnification.

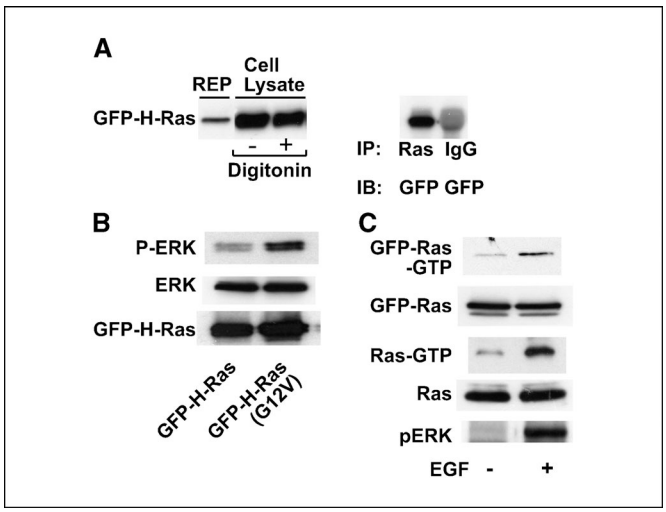

Figure 5. Rasosomes act as a signaling platform. *A,* GFP-H-Ras(G12V)–transfected COS cells were permeabilized with digitonin or left untreated as detailed in Materials and Methods. The medium of the digitonized cell was collected and used for the preparation of a REP. REP and lysates of the untreated cells and of the digitonized cells equivalent respectively to 4.5×10^4, 1.5×10^4, and 1.5×10^4 cells were then assayed by Western immunoblotting (*IB*) with anti-GFP antibody (*left*). REP, equivalent to 4.5×10^5 cells, was also subjected to immunoprecipitation (*IP*) with pan-Ras antibody or with naive rat IgG followed by Western immunobloting with anti GFP antibody (*right*) *B,* REPs of GFP-H-Ras or GFP-H-Ras(G12V) transfectants were immunoprecipitated by pan-Ras antibody beads, which where then assayed by Western immunoblotting with anti–phospho-ERK antibodies. Total ERK and GFP-Ras served as the transfection control. *C,* REPs of control and EGF-stimulated GFP-H-Ras transfectants were pulled down by GST-RBD for determination of GFP-Ras-GTP and endogenous Ras-GTP or were immunoprecipitated by pan-Ras antibody beads for determination of phospho-ERK on the rasosomes. Total GFP-Ras and total endogenous Ras in the transfectants are also shown.

digitonized cells do not represent GFP-H-Ras(G12V) protein associated with plasma membrane debris. Second, we collected GFP-labeled particles from the media of digitonized GFP-H-Ras(G12V) transfectants as follows. We removed cell debris and heavy membranes by a 20,000 $\times$ *g* centrifugation step. We then subjected the 20,000 $\times$ *g* supernatant to ultracentrifugation at 100,000 $\times$ *g* to precipitate the particles and to remove soluble GFP-H-Ras(G12V). We then trapped the particles of this preparation (rasosome enriched preparation, REP) either on GFP antibody (data not shown) or on Ras antibody beads (Fig. 4*B*). The particles appeared as diffraction-limited fluorescent spots on the beads, similar to those observed in the live cells. No particles were detected on control naïve IgG beads that were incubated with GFP-H-Ras(G12V) particles (Fig. 4*B*). Third, we subjected GFP-H-Ras(G12V) particles that were trapped on Ras antibody beads to high-resolution SEM. The particles attached to the beads appeared as round structures with diameter of 80 to 100 nm (Fig. 4*C*) that were not present on control antibody beads (data not shown). These experiments enabled us to characterize the rasosome as a nanometric particle that carries palmitoylated Ras proteins. Fourth, in line with the observations that only a relatively small fraction of the total cellular GFP-H-Ras is detected in rasosomes (Fig. 1*A*), we detected by immunoblotting a very small fraction of GFP-H-Ras(G12V) in the REP (Fig. 5*A*). GFP-H-Ras (G12V) in the REP corresponded to 1.5 $\pm$ 1% (n = 3) of that found in the total cell lysate; GFP-H-Ras(G12V) that remained in the cells after the digitonization was indeed not significantly different from that found before the treatment corresponded (Fig. 5*A*). GFP-H-Ras(G12V) loaded rasosomes of the REP could be specifically immunoprecipitated by the Ras antibody (Fig. 5*A*).

Extracellular signal induces activation of rasosome-associated GFP-H-Ras and ERK. Based on the estimated size of the rasosome, it can accommodate multiple copies of Ras as well as additional protein molecules. This, along with the data demonstrating that the constitutively active H-Ras(G12V) interacts with rasosomes, suggested that the rasosome might act as a carrier of Ras signaling complexes. To examine this possibility, we isolated rasosomes from both GFP-H-Ras and GFP-H-Ras(G12V) transfectants, trapped them on Ras antibody beads, and subjected the immunoprecipitated rasosomes to immunoblotting with antibody against active phospho-ERK, a downstream target of active Ras (1). Because phospho-ERK was detected mainly in rasosomes carrying GFP-H-Ras(G12V) (Fig. 5*B*), we postulated that rasosomes respond to extracellular stimuli that activate Ras. To examine this possibility, we stimulated GFP-H-Ras transfectants with 100 nmol/L EGF for 3 minutes, then isolated rasosomes and incubated them with the Ras-binding domain of Raf (RBD)-GST fusion protein attached to glutathione beads to trap the active GFP-H-Ras. We found that EGF induced an increase both in the rasosome-associated GFP-H-Ras-GTP and in phospho-ERK (Fig. 5*C*). Importantly, we also found that EGF induced increase in GTP loading of the endogenous Ras associated with the GFP-Ras rasosome preparation (Fig. 5*C*). These experiments strongly suggested that the endogenous Ras proteins, like the GFP-tagged palmitoylated Ras proteins, are associated with rasosomes. The presence of active ERK along with Ras-GTP in the rasosome suggests that the rasosome carries signaling molecules and can act as a platform for transmission of signals across the cytoplasm.

Conclusions. The experiments described here enabled us to define a hitherto unknown cellular signaling nanoparticle, the rasosome, which moves rapidly in an ATP-independent random motion in the cytosol and carries multiple copies of palmitoylated Ras proteins. The association of H-Ras and N-Ras with rasosomes requires Ras palmitoylation and the hvr domain. H-Ras hvr mutants that fail to interact with rasosomes are biologically inactive. Cytoplasmic H-Ras rasosomes can become immobilized at the plasma membrane and can receive extracellular signals leading to the appearance of cytoplasmic "activated rasosomes" loaded with H-Ras-GTP and active ERK; these rasosomes can then transmit the signal through the cytoplasm. The rasosome thus provides a means whereby palmitoylated Ras can be transmitted to and from the plasma membrane, promoting the rapid spread of Ras signal information across the cell. Additional proteins that are likely to be present in the rasosomes are Raf, the Ras scaffold protein KSR and mitogen-activated protein/ERK kinase. It is also possible that other effectors are present in the rasosomes as well as palmitoylated proteins other than Ras (e.g., caveolin; refs. 37, 38; or Wrch; ref. 39).

Acknowledgments

Received 10/20/2005; revised 12/14/2005; accepted 12/20/2005.

Grant support: The Israel Science Foundation grants 339/02-3 (Y. Kloog) and 424/02-16.6 (U. Ashery), the Wolfson Family Foundation Trust (Y. Kloog), and the Minerva Junior Research Group (U. Ashery).

The costs of publication of this article were defrayed in part by the payment of page charges. This article must therefore be hereby marked *advertisement* in accordance with 18 U.S.C. Section 1734 solely to indicate this fact.

We thank S.R. Smith for editorial assistance and Zahava Barkay of the Tel Aviv University Wolfson Applied Materials Research Center for SEM assistance.

References

1. Downward J. Targeting RAS signalling pathways in cancer therapy. Nat Rev Cancer 2003;3:11–22.
2. Bar-Sagi D, Hall A. Ras and Rho GTPases: a family reunion. Cell 2000;103:227–38.
3. Malumbres M, Barbacid M. RAS oncogenes: the first 30 years. Nat Rev Cancer 2003;3:459–65.
4. Cox AD, Der CJ. The dark side of Ras: regulation of apoptosis. Oncogene 2003;22:8999–9006.
5. Niv H, Gutman O, Kloog Y, Henis YI. Activated K-Ras and H-Ras display different interactions with saturable nonraft sites at the surface of live cells. J Cell Biol 2002; 157:865–72.
6. Niv H, Gutman O, Henis YI, Kloog Y. Membrane interactions of a constitutively active GFP-Ki-Ras 4B and their role in signaling. Evidence from lateral mobility studies. J Biol Chem 1999;274:1606–13.
7. Prior IA, Muncke C, Parton RG, Hancock JF. Direct visualization of Ras proteins in spatially distinct cell surface microdomains. J Cell Biol 2003;160:165–70.
8. Rotblat B, Prior IA, Muncke C, et al. Three separable domains regulate GTP-dependent association of H-ras with the plasma membrane. Mol Cell Biol 2004;24: 6799–810.
9. Lommerse PH, Snaar-Jagalska BE, Spaink HP, Schmidt T. Single-molecule diffusion measurements of H-Ras at the plasma membrane of live cells reveal microdomain localization upon activation. J Cell Sci 2005;118: 1799–809.
10. Murakoshi H, Iino R, Kobayashi T, et al. Single-molecule imaging analysis of Ras activation in living cells. Proc Natl Acad Sci U S A 2004;101:7317–22.
11. Philips MR. Compartmentalized signalling of Ras. Biochem Soc Trans 2005;33:657–61.
12. Jiang X, Sorkin A. Coordinated traffic of Grb2 and Ras during epidermal growth factor receptor endocytosis visualized in living cells. Mol Biol Cell 2002;13:1522–35.
13. Plowman SJ, Hancock JF. Ras signaling from plasma membrane and endomembrane microdomains. Biochim Biophys Acta 2005;1746:274–83.
14. Rocks O, Peyker A, Kahms M, et al. An acylation cycle regulates localization and activity of palmitoylated Ras isoforms. Science 2005;307:1746–52.
15. Roy S, Plowman S, Rotblat B, et al. Individual palmitoyl residues serve distinct roles in h-ras trafficking, microlocalization, and signaling. Mol Cell Biol 2005; 25:6722–33.
16. Goodwin JS, Drake KR, Rogers C, et al. Depalmitoylated Ras traffics to and from the Golgi complex via a nonvesicular pathway. J Cell Biol 2005;170:261–72.
17. Jaumot M, Yan J, Clyde-Smith J, Sluimer J, Hancock JF. The linker domain of the Ha-Ras hypervariable region regulates interactions with exchange factors, Raf-1 and phosphoinositide 3-kinase. J Biol Chem 2002;277: 272–8.
18. Gasparini L, Benussi L, Bianchetti A, et al. Energy metabolism inhibition impairs amyloid precursor protein secretion from Alzheimer's fibroblasts. Neurosci Lett 1999;263:197–200.
19. Navarro-Lerida I, Corvi MM, Barrientos AA, et al. Palmitoylation of inducible nitric-oxide synthase at Cys-3 is required for proper intracellular traffic and nitric oxide synthesis. J Biol Chem 2004;279:55682–9.
20. Saxton MJ, Jacobson K. Single-particle tracking: applications to membrane dynamics. Annu Rev Biophys Biomol Struct 1997;26:373–99.
21. Gonzales R, Woods RE. Digital image processing. MA: Wesley, Reading; 1993.
22. Axelrod D. Total internal reflection fluorescence microscopy in cell biology. Traffic 2001;2:764–74.
23. Campbell RE, Tour O, Palmer AE, et al. A monomeric red fluorescent protein. Proc Natl Acad Sci U S A 2002; 99:7877–82.
24. Choy E, Chiu VK, Silletti J, et al. Endomembrane trafficking of ras: the CAAX motif targets proteins to the ER and Golgi. Cell 1999;98:69–80.
25. Lang T, Wacker I, Steyer J, et al. Ca^{2+}-triggered peptide secretion in single cells imaged with green fluorescent protein and evanescent-wave microscopy. Neuron 1997;18:857–63.
26. Colicos MA, Collins BE, Sailor MJ, Goda Y. Remodeling of synaptic actin induced by photoconductive stimulation. Cell 2001;107:605–16.
27. Oheim M, Loerke D, Stuhmer W, Chow RH. The last few milliseconds in the life of a secretory granule. Docking, dynamics and fusion visualized by total internal reflection fluorescence microscopy (TIRFM). Eur Biophys J 1998;27:83–98.
28. Li CH, Bai L, Li DD, Xia S, Xu T. Dynamic tracking and mobility analysis of single GLUT4 storage vesicle in live 3T3-L1 cells. Cell Res 2004;14:480–6.
29. Li D, Xiong J, Qu A, Xu T. Three-dimensional tracking of single secretory granules in live PC12 cells. Biophys J 2004;87:1991–2001.
30. Goulian M, Simon SM. Tracking single proteins within cells. Biophys J 2000;79:2188–98.
31. Bergmann JE, Trachsel H, Sonenberg N, Shatkin AJ, Lodish HF. Characterization of rabbit reticulocyte factor(s) that stimulates the translation of mRNAs lacking 5′-terminal 7-methylguanosine. J Biol Chem 1979; 254:1440–3.
32. Yamashiro DJ, Maxfield FR. Acidification of endocytic compartments and the intracellular pathways of ligands and receptors. J Cell Biochem 1984;26:231–46.
33. Punnonen EL, Ryhanen K, Marjomaki VS. At reduced temperature, endocytic membrane traffic is blocked in multivesicular carrier endosomes in rat cardiac myocytes. Eur J Cell Biol 1998;75:344–52.
34. Hancock JF, Paterson H, Marshall CJ. A polybasic domain or palmitoylation is required in addition to the CAAX motif to localize p21ras to the plasma membrane. Cell 1990;63:133–9.
35. Coleman RA, Rao P, Fogelsong RJ, Bardes ES. 2-Bromopalmitoyl-CoA and 2-bromopalmitate: promiscuous inhibitors of membrane-bound enzymes. Biochim Biophys Acta 1992;1125:203–9.
36. Krause KH, Fivaz M, Monod A, van der Goot FG. Aerolysin induces G-protein activation and Ca^{2+} release from intracellular stores in human granulocytes. J Biol Chem 1998;273:18122–9.
37. Pelkmans L, Zerial M. Kinase-regulated quantal assemblies and kiss-and-run recycling of caveolae. Nature 2005;436:128–33.
38. Tagawa A, Mezzacasa A, Hayer A, et al. Assembly and trafficking of caveolar domains in the cell: caveolae as stable, cargo-triggered, vesicular transporters. J Cell Biol 2005;170:769–79.
39. Berzat AC, Buss JE, Chenette EJ, et al. Transforming activity of the Rho family GTPase, Wrch-1, a Wnt-regulated Cdc42 homolog, is dependent on a novel carboxyl-terminal palmitoylation motif. J Biol Chem 2005;280:33055–65.

Ras and Its Signals Diffuse through the Cell on Randomly Moving Nanoparticles

Barak Rotblat, Ofer Yizhar, Roni Haklai, et al.

Cancer Res 2006;66:1974-1981.